Research Paper

Journal of Engineering and Technological Sciences

Tailoring BiOBr Photocatalyst: In-situ Bi Doping for Enhanced Photocatalytic Removal of Sulfamethoxazole (SMX) Antibiotic

Sabrina Prima Fauziyen[1], Wibawa Hendra Saputera[1,2,3,*] & Dwiwahju Sasongko[1,3]

[1]Research Group on Sustainable Energy and Technology, Department of Chemical Engineering, Faculty of Industrial Technology, Institut Teknologi Bandung, Jalan Ganesa No. 10, Bandung, 40132, Indonesia
[2]Center for Catalysis and Reaction Engineering, Institut Teknologi Bandung, Jalan Ganesa No. 10, Bandung, 40132, Indonesia
[3]Research Center for New and Renewable Energy, Institut Teknologi Bandung, Jalan Ganesa No. 10, Bandung, 40132, Indonesia

*Corresponding author: whsaputera@itb.ac.id

Abstract

There is a notable emphasis on the development of photocatalysts to degrade antibiotics, such as sulfamethoxazole (SMX), in aquatic environments due to their persistence and associated toxicological impacts. In this study, BiOBr photocatalysts were synthesized by incorporating in-situ Bi doping. Various Bi/BiOBr composites were produced through a hydrothermal method at varying temperatures and subsequently characterized using X-ray diffraction (XRD), UV-vis diffuse reflectance spectroscopy (UV-vis DRS), X-ray fluorescence (XRF), and nitrogen adsorption-desorption isotherm. The characterization data revealed that the Bi-metal began to emerge at a hydrothermal temperature of 180 °C (BB180) in the BiOBr-based semiconductor and completed its conversion to Bi-metal at a hydrothermal temperature of 270 °C (BB270). This transformation leads to the generation of Bi^{3+} in conjunction with oxygen vacancies, acting as active electron traps and enhancing the separation efficiency of light-induced electron-hole pairs. This results in a narrow band gap of Bi/BiOBr photocatalyst, increasing its sensitivity towards visible light. BB180 exhibited the highest photocatalytic rate in the degradation of SMX with a removal efficiency of 74.35% within 4 hours of reaction under Xenon lamp irradiation and an apparent rate constant of 6.5 x 10^{-3} min^{-1}, surpassing the commercial TiO_2 Degussa P25. This finding opens up a new pathway for the development of a catalyst responsive to visible light, specifically designed for the detoxification of antibiotics in wastewater.

Keywords: *Bi/BiOBr; hydrothermal; in-situ Bi doping; photocatalytic; sulfamethoxazole.*

Introduction

Sulfamethoxazole (SMX), an antibiotic in the sulfonamide class, has been identified as a new micropollutant. It is commonly used in human and veterinary medicine to treat different types of infectious diseases. The residues of SMX have a long-lasting presence in the environment and are classified as persistent antibiotics, leading to toxicological impacts [1,2]. Studies have revealed that SMX poses a significant environmental risk even at low concentrations by causing changes in the microbial community structure and promoting antibiotic resistance development. This pollutant can enter water bodies, including drinking water sources, through various routes, such as improper pharmaceutical waste disposal, toilet flushing, and fecal contamination [3,4].

The utilization of photocatalytic technology has emerged as a promising technology for eliminating and breaking down antibiotics in water sources. The effectiveness of this process relies on the implementation of photocatalysts. Significant advancements have been made in developing semiconductor-based photocatalysts in recent years [5-7], with particular attention given to bismuth oxyhalide-based photocatalysts. These photocatalysts belong to a new category of layered materials that exhibit promising photocatalytic energy conversion and environmental remediation capabilities. Extensive research has been conducted on the application and physiochemical properties of BiOX photocatalysts [8-13]. Bismuth oxybromide (BiOBr) has gained considerable attention due to its favorable activity and stability when exposed to visible light. BiOBr

ISSN: 2337-5779
J. Eng. Technol. Sci. Vol. 56, No. 2, 2024, 266-274
DOI: 10.5614/j.eng.technol.sci.2024.56.2.7

DOI: 10.5614/j.eng.technol.sci.2024.56.2.7

possesses a layered structure characterized by the arrangement of $(Bi_2O_2)^{2+}$ plates alternating with Br double plates [14].

To address the limitations of pure BiOX photocatalysts, such as their high electron-hole recombination rate and limited surface adsorption capacity, researchers have explored various strategies to enhance their photocatalytic performance. One practical approach is the incorporation of noble metals into BiOX (Cl, Br and I) to achieve a uniform structure. For instance, a study conducted by Yu *et al.* [15] demonstrated that adding noble metal particles, such as Rh, Pd and Pt, significantly improves the photocatalytic activity of BiOX. This enhancement can be attributed to the strong absorption of visible light and the reduced recombination rate of electron-hole pairs facilitated by the presence of noble metal particles. However, the use of noble metals can be cost-prohibitive. Therefore, an alternative approach involves the utilization of transition metals in the design of metal-containing photocatalysts based on BiOBr, aiming to replace the expensive noble metals while maintaining desirable photocatalytic properties and performance.

Hence, we opted to employ a strategy that involves integrating Bi-metal within the hierarchical structure of BiOBr to enhance the photocatalytic activity. Several studies have explored the application of Bi/BiOBr in the photodegradation of textile waste, particularly dyes. The outcomes of these studies indicated that these photocatalysts effectively reduce the recombination rate of electron-hole pairs and increase light absorption through surface plasmon resonance (SPR) phenomena [16-18]. In line with the earlier research conducted by Cao *et al.* [19], the present study followed a similar approach to preparing the Bi/BiOBr photocatalyst. We employed diethylene glycol (DEG) as a reaction medium to facilitate the in-situ reduction and growth of Bi nanoparticles on the surface of BiOBr. This method helps to prevent the aggregation of zero-dimensional nanoparticles, resulting in the creation of more active sites for enhanced photocatalytic performance.

In this study, we introduced polyvinylpyrrolidone (PVP) as a modifying agent in the hydrothermal process to exert precise control over the structure, shape, and size of the nanoparticles [20]. This approach enabled us to successfully synthesize Bi/BiOBr nanoparticles with a narrow band gap and an optimized exposed surface area. By adjusting the hydrothermal process temperatures of 150, 180, 210, 240 and 270 ℃, we achieved the desired characteristics in the prepared nanoparticles.

Materials and Methods

Synthesis of Bi/BiOBr

All chemicals utilized in this study were analytical grade and did not undergo additional purification steps. The experimental procedure involved several stages. Initially, a solution, designated as solution A, was prepared by dissolving 5 moles of KBr (100%, Sigma Aldrich) in 50 ml of diethylene glycol (DEG, 100%, Sigma Aldrich). Subsequently, solution B was prepared by dissolving 5 moles of $Bi(NO_3)_3.5H_2O$ (99%, Xilong Scientific) and 0.2 grams of polyvinylpyrrolidone (PVP, 100%, Sigma Aldrich) in 50 ml of DEG.

Solution B was added to solution A while stirring the mixture for 20 minutes using a magnetic stirrer. The resulting mixture was then transferred and sealed within an autoclave for hydrothermal treatment, with temperature variations of 150, 180, 210, 240 and 270 ℃ for 12 hours. After completion, the autoclave was allowed to cool naturally. Subsequently, the precipitate was separated and washed to obtain the desired solid. The precipitate was then dried at 60 ℃ for 6 hours, resulting in the formation of Bi/BiOBr powder. Samples were labeled BBX, where X is the temperature of hydrothermal treatment.

Characterization of Bi/BiOBr

XRD (X-ray diffraction) analysis was carried out using a Bruker D8 Advance (Bruker Corporation, Billerica, MA, USA) to examine the crystal phase composition of BiOBr and the presence of Bi metal. The data was collected in the 2θ range of 10° to 90° with a step size of 0.020°. The diffractometer was equipped with a Cu Kα radiation source (λ = 1.5406 Å). The obtained diffraction patterns were processed using X'Pert High Score and OriginLab

software. To assess the optical properties and determine the band gap of the BiOBr-based catalyst, UV-vis diffuse reflectance spectroscopy (UV-Vis DRS, UV-Vis Thermo Fischer Scientific Evolution 220, USA) was employed.

$BaSO_4$ was utilized as a reference material during the measurements. The band gap measurement was calculated based on the Kubelka-Munk equation, $\alpha h\nu = A(h\nu - Eg)^{n/2}$, where υ, h, α, and A represent the frequency of light, Planck's constant, the absorption coefficient, band gap, and proportionality constant, respectively [21]. X-ray fluorescence (XRF EDAX ORBIS Vision, USA) was used to identify the elements in samples of synthesized Bi/BiOBr catalysts. The specific surface area, pore volume and average pore size of the catalyst were determined using the Nova Touch LUX 4 device and the BET (Brunauer-Emmet-Teller) method.

Photocatalytic Activity Assessment

The photocatalytic degradation of SMX was conducted in a Pyrex reactor using a 300 W Xenon lamp as the light source, emitting wavelengths between 200 and 1,000 nm; a 350-ml solution containing 100 mg/L SMX was prepared in the reactor. Various photocatalysts (BB150, BB180, BB210, BB240, and BB270) were added to the solution at a concentration of 800 mg/L and stirred for 60 minutes to achieve adsorption equilibrium. Subsequently, the solution was sonicated to ensure homogeneous dissolution and equalize the particle size of the catalyst. Simultaneously, pure O_2 was allowed to flow continuously into the photoreactor as the source of reactive oxygen species (ROS) generation. Once the system achieved equilibrium, the light source was turned on and the photocatalytic process was carried out for 4 hours. At 40-minute intervals, 10 ml of the samples were taken for analysis. Prior to analysis, the solution was transformed into a complex solution by dissolving it in a mixture comprising 5.5 ml of 10% ethanol (100%, Sigma Aldrich) and 10 ml of sodium acetate–acetic acid buffer solution (pH = 4.5) in a 25-ml volumetric flask.

The concentration of SMX in the samples was determined using a UV-Vis Shimadzu 1800 double-beam spectrophotometer, with a maximum wavelength set at 268 nm. The reaction rate constants were calculated to evaluate the photocatalytic performance of these samples and determine the rate at which SMX undergoes degradation through photocatalysis. The kinetic rate constant was calculated using the first-order kinetic ratio expressed in the equation $-\ln\frac{C}{C_0} = kt$, where C_0 is the initial concentration of SMX, C is the concentration at a given time, and k is the first-order reaction rate constant [22].

Results and Discussion

XRD characterization was conducted to examine the purity and phase structure of the synthesized catalyst samples. Figure 1 (a) illustrates the nanostructures of samples BB150, BB180, BB210, and BB240, revealing distinct reflection peaks with specific 2θ angles. These peaks were identified as follows: 31.8˚, 32.3˚, 46.3˚, 57.3˚, 67.6°, and 76.9°, corresponding to planes (012), (110), (020), (212) (220), and (130) respectively. These findings indicate the presence of a tetragonal phase of BiOBr (JCPDS No. 01-073-2061) with a space group of *P*4/*nmm* (129). Notably, in samples BB180, BB210, BB240 and BB270, additional diffraction peaks were observed at 2θ of 23.7°, 27.1°, 37.9°, 39.6°, 44.6°, 48.7°, 56.1°, 62.2°, 64.5°, 67.4°, 70.7°, 71.9°, 85.3° and 89.5˚ corresponding to planes (101), (012), (104), (110), (015), (202), (024), (116), (122), (018), (214), (300), (220) and (306) respectively, and are indexed to Bi metal (JCPDS No. 00-005-0519).

The XRD pattern results indicate that the synthesis temperature has an impact on the number of peaks produced, specifically the Bi-metal peak. At a synthesis temperature of 270 ℃(BB270), the peak is dominated by Bi-metal, and the tetragonal phase peak from BiOBr is no longer present. The pronounced intensity and sharpness of the diffraction peaks observed in the Bi/BiOBr nanostructure signify a high level of crystallinity in its crystal structure. This is corroborated by the XRD findings, which reveal crystallinity percentages of 50.9%, 57.2%, 58.5%, 78.5%, and 87.3% for samples BB150, BB180, BB210, BB240, and BB270, respectively. Hence, it can be concluded that the percentage of crystallinity rises proportionally with an increase in synthesis temperature.

DOI: 10.5614/j.eng.technol.sci.2024.56.2.7

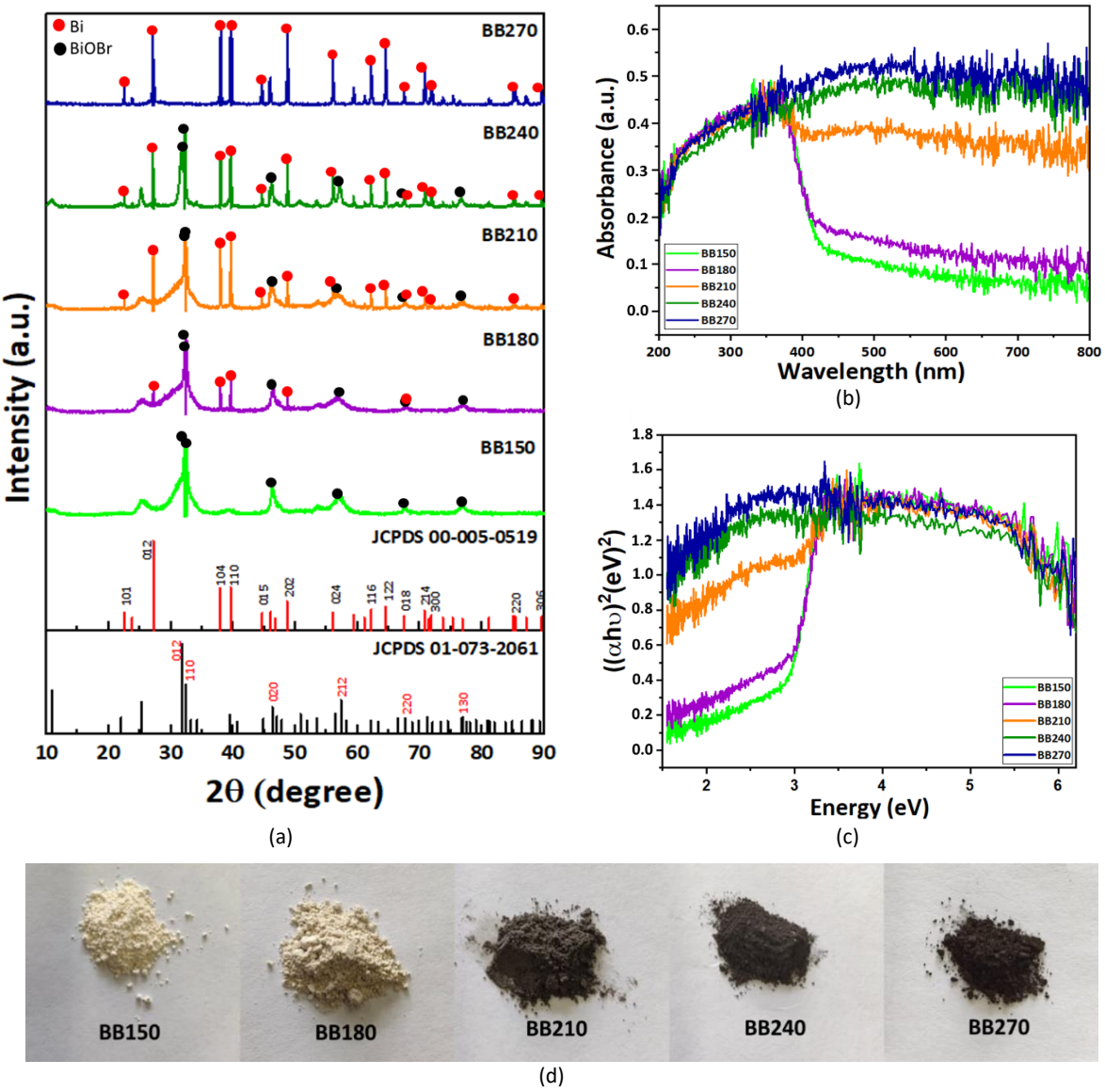

Figure 1 (a) XRD patterns of Bi/BiOBr with different hydrothermal synthesis temperatures in comparison with the BiOBr and Bi-metal peaks from JCPDS; (b) UV-Vis diffuse reflectance spectra; (c) Kubelka-Munk plots, $(\alpha h\nu)^{1/2}$ to photon energy $(h\nu)$ for the band gap energy calculation for Bi/BiOBr samples with different hydrothermal reaction temperatures; (d) visual appearances of synthesized BB150, BB180, BB210, BB240, BB270 catalysts.

The introduction of Bi through in-situ doping enhances the dissociation of Bi^{3+} ions in BiOBr due to the relatively low stability constant of BiOBr ($K_{sp} = 3 \times 10^{-7}$). This facilitates the reduction of Bi^{3+} ions to metallic Bi. In the synthesis process of Bi/BiOBr, DEG serves not only as a solvent but also as a reducing agent. DEG has the capability to coordinate with Bi^{3+} ions, forming a homogeneous precursor that subsequently decomposes at elevated temperatures (220 °C) [23]. Owing to the high stability constant, DEG partially reduced Bi^{3+} to Bi within the BiOBr system. The significance of high and low stability constants becomes evident in the partial reduction of Bi^{3+} to Bi. In coordination chemistry, stability constants measure the strength of the interactions between metal ions and ligands. Elevated stability constants signify a robust interaction, proving advantageous for creating enduring complexes. In the realm of bismuth (III) complexation, a heightened appreciation of stability constants is essential for comprehending the potent binding of Bi^{3+} to ligands. This is exemplified by the remarkably sturdy complexes formed with natural organic matter. Conversely, lower stability constants may influence the development of distinct bismuth species under specific pH conditions [24]. In the BB150 sample, due to the low reaction temperature Bi-metal is not formed, resulting in a composition predominantly consisting

of BiOBr. As the hydrothermal reaction temperature increases, the formation of Bi metal becomes more evident. In the BB270 sample, Bi-metal dominates the composition as the Bi^{3+} ions have been successfully reduced to Bi.

The UV-vis diffuse reflectance spectra of the samples were analyzed within the wavelength range of 200~800 nm, as shown in Figure 1(b). Samples BB150 and BB180 exhibited higher UV light absorption than visible light. In the visible light region, the samples showed a noticeable decrease in light absorption as the wavelength increased. However, as the hydrothermal reaction temperature increased, the Bi/BiOBr composites (BB210, BB240 and BB270) demonstrated significantly enhanced light absorption, particularly in the visible light range. This was evident by the change in color of the samples: BB150 and BB180 appeared white-gray, while BB210, BB240 and BB270 appeared gray-black. The darker color of the samples at higher hydrothermal reaction temperatures indicated increased light absorption throughout the measurement wavelength range, attributed to the occurrence of surface plasmon resonance [25].

The determination of the band gap can be estimated by plotting the band gap through $(\alpha h\nu)^{1/2}$ curve to the photon energy $(h\nu)$ using the Kubelka-Munk function. In the Kubelka-Munk equation, the value of n is set to 4 for indirect and 1 for direct transitions. For the BiOBr material, a value of 4 is assigned to n, indicating an indirect transition [26]. Based on Figure 1(c), it can be observed that the estimated band gap values for BB150 and BB180 samples are 2.79 eV and 2.74 eV, respectively. However, the band gaps for BB210, BB240, and BB270 samples are too small to define precisely. It is worth noting that the band gap energy of BB180 is smaller than that of BB150, which enhances the absorption of visible light and promotes photocatalytic reactions due to the abundant oxygen vacancies present in the Bi/BiOBr composite [16].

The results of the photocatalytic degradation of SMX pharmaceutical waste using the synthesized catalysts are presented in Figure 2. The comparison of photocatalytic activity among BB150, BB180, BB210, BB240 and BB270 is shown in Figure 2(b). Within 4 hours, BB150 achieved a 69.00% degradation of SMX under UV-visible light irradiation. Similarly, BB180 exhibited the highest degradation rate among all samples, reaching 74.35%. On the other hand, BB210, BB240 and BB270 demonstrated respective degradation rates of 69.53%, 62.69% and 62.26%. These findings indicate that increasing the hydrothermal reaction temperature does not enhance the photocatalytic activity trend. Based on the XRD results (Figure 1(a)), there is a growing dominance of the Bi-metal composition in the synthesized samples as the hydrothermal reaction temperature rises. This observation is supported by the XRF results, indicating Bi compositions of 73.5%, 75.4%, 77.88%, 80.45%, 99.74% for samples BB150, BB180, BB210, BB240, and BB270, respectively. In addition, as indicated by the UV-vis diffuse reflectance spectrum (Figures 1(b) and 1(c)), there is a notable increase in the absorption of visible light, leading to a less effective performance of the catalyst sample since the light source employed in this experiment was UV-vis light. To provide a comparative analysis, the photocatalytic performance of TiO_2 Degussa P25 was also explored as a control experiment. The outcomes revealed that the degradation of SMX was comparatively slower in TiO_2 compared to catalyst BB180. The photocatalytic activity test results indicate that TiO_2 can degrade SMX by up to 66.57% in 4 hours under UV-vis irradiation.

Table 1 Specific surface area, pore volume and pore size of catalysts BB150, BB180, BB210, BB240, and BB270.

Photocatalyst	Specific surface area (m^2/g)	Pore volume (cm^3/g)	Average pore radius (nm)
BB150	12.29	0.0216	6.71
BB180	32.78	0.0322	3.23
BB210	10.24	0.0251	8.83
BB240	13.34	0.0090	1.91
BB270	4.25	0.0055	5.61

Figure 2 (b) shows the kinetic rate constant of the catalyst, which provides a deeper understanding of the activity of the catalytic system. The calculated reaction rate constants of SMX photodegradation for each catalyst were as follows: 0.0057 min^{-1} for BB150, 0.0065 min^{-1} for BB180, 0.0057min^{-1} for BB210, 0.0051 min^{-1} for BB240 and 0.0049 min^{-1} for BB270. Under UV-visible light irradiation, BB180 showed the highest reaction rate constant and, hence, the highest photocatalytic performance compared to the other photocatalysts. According to the surface area analysis, BB180 exhibited the highest surface area of 32.78 m^2/g, surpassing the other samples with surface

DOI: 10.5614/j.eng.technol.sci.2024.56.2.7

areas of 12.29 m^2/g, 10.24 m^2/g, 13.34 m^2/g, and 4.25 m^2/g for BB150, BB210, BB240, and BB270, respectively (Table 1). This substantial surface area can lead to enhanced separation of electron and holes, improved light absorption, and reduction in recombination sites, collectively contributing to an augmented photocatalytic activity [27].

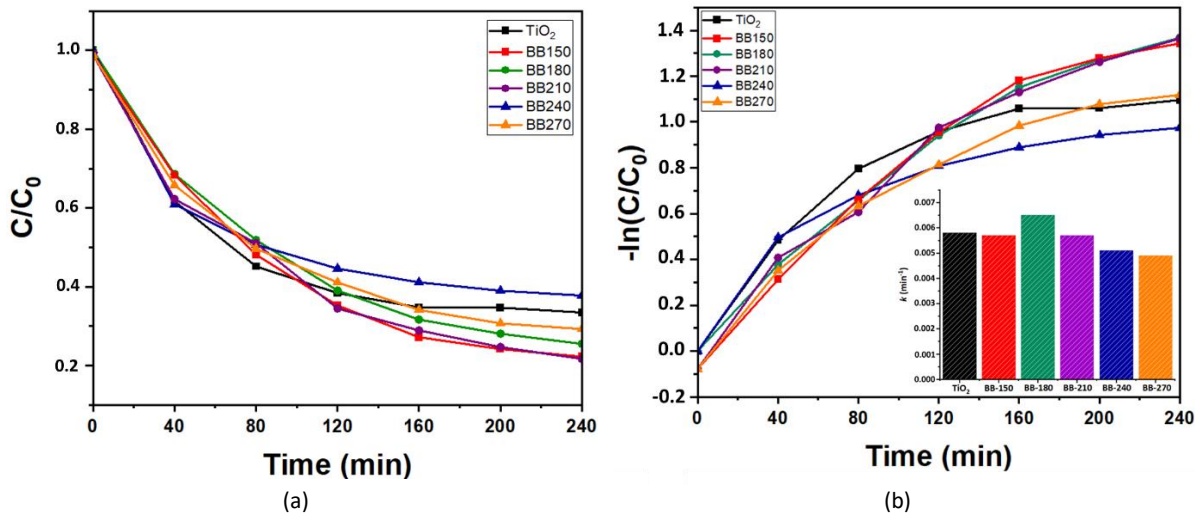

(a) (b)

Figure 2 (a) Photocatalytic degradation of SMX; (b) the pseudo first order reaction kinetics and corresponding photocatalytic degradation efficiencies (inset) using Bi/BiOBr catalysts and TiO_2 Degussa P25.

To assess the photocatalytic efficiency of Bi/BiOBr composites in degrading SMX, Table 2 compares the reaction rate constants between the synthesized Bi/BiOBr and other previously reported photocatalysts.

Table 2 Comparison of various catalysts for photocatalytic degradation of SMX.

Photocatalyst	Operating Conditions			Band Gap Energy (eV)	k (min^{-1})	Reference
	$[SMX]_0$ (ppm)	Light source	Reaction time			
Bi/BiOBr	50	Xe lamp 300 W	240 min	2.74	6.5×10^{-3}	This study
g-C_3N_4	1	Xe lamp 300 W	60 min	2.93	3.0×10^{-3}	[28]
Er^{3+}/Tb^{3+}@BiOBr	10	Tungsten Halogen 500 W	72 min	2.78	7.1×10^{-3}	[12]
g-C_3N_5	10	Tungsten Halogen 500 W	72 min	2.18	4.5×10^{-3}	
$BiVO_4$	5	Xe lamp 300 W	90 min	2.44	1.93×10^{-4}	[29]
BiOCl	5	Xe lamp 300 W	90 min	3.54	2.12×10^{-3}	
BiOCl/$BiVO_4$ p-n heterojunction	5	Xe lamp 300 W	90 min	n.a.	6.68×10^{-3}	
Bi_2O_3	10	Solar simulator 300 W	180 min	2.81	7.0×10^{-3}	[30]
TiO_2 pure brookite	10	UV-A fluorescent 90 W	180 min	n.a.	3.0×10^{-3}	[31]
$AgNbO_3$	10	Fluorescent	720 min	2.71	5.0×10^{-3}	[32]

Previous studies have suggested that oxygen vacancies have the capability to attract impurity levels within the range of the valence band (VB) and the conduction band (CB) [6,33]. Consequently, the BB180 sample exhibited a narrow band gap, rendering it highly responsive to visible light. When exposed to light energy surpassing the band gap, electrons undergo transfer from the VB to the CB in BiOBr or the oxygen vacancies, resulting in the

generation of electron-hole pairs. The presence of oxygen, serving as an active electron trap, amplifies the separation efficiency of these light-induced electron-hole pairs, leading to a notably elevated level of photocatalytic activity. In addition, based on the XRD results (Figure 1(a)), it is evident that the sample exhibited a composition with a good balance between Bi-metal and BiOBr, with the Bi-metal being present on the surface of the photocatalyst. Consequently, during the photoreaction process, the Bi-metal acts as an electron scavenger, promoting the preferential transfer of electrons induced by light to the Bi-metal instead of recombination with the holes induced by light. This results in a reduced likelihood of charge pair recombination, ultimately hindering the photocatalytic reaction [16].

Conclusion

In this study, Bi/BiOBr photocatalysts were successfully synthesized through the hydrothermal method. The investigation focused on the impact of hydrothermal synthesis reaction temperature, ranging from 150 to 270 ℃, on the alteration of crystal structure, specific surface area, elemental composition, and band gap values. The photocatalytic performance of Bi/BiOBr was assessed by studying the degradation of SMX under UV-visible light. The results revealed that BB180 exhibited the highest photocatalytic activity, achieving a removal efficiency of 74.35% and an apparent rate constant of 6.5×10^{-3} min^{-1}. This enhanced photocatalytic performance is attributed to the optimum band gap value (2.74 eV), highest surface area (32.74 m^2/g), and the presence of metal Bi and oxygen vacancies within the BiOBr-based semiconductor, serving as active electron traps, leading to improved separation efficiency of light-induced electron-hole pairs. This discovery provides a novel approach for developing a catalyst that responds to visible light, aiming to detoxify antibiotics in wastewater.

Acknowledgment

This work was supported by an Asahi Glass Foundation Overseas Research Grant 2022-2023 (Grant No. 1422/IT1.B07.1/TA.00/2022 and 1647/IT1.B07.1/TA.00/2023) and a grant from the Indonesian Ministry of Education, Culture, Research, and Technology Research Program 2023 (Grant No. 110/E5/PG.02.00/PL/2023). All material characterizations were carried out at the Research Center for Nanoscience and Nanotechnology, ITB.

References

[1] Dirany, A., Aaron, S.E., Oturan, N., Sirés, I., Oturan, M.A. & Aaron, J.J., *Study of The Toxicity of Sulfamethoxazole and Its Degradation Products in Water by a Bioluminescence Method During Application of the Electro-Fenton Treatment*, Anal Bioanal Chem, **400**, pp. 353-360, Nov. 2011.

[2] Kim, J.R. & Kan, E., *Heterogeneous Photocatalytic Degradation of Sulfamethoxazole in Water Using a Biochar-Supported TiO_2 Photocatalyst*, Journal of Environmental Management, **180**, pp. 94-101, May. 2016.

[3] Ding, S., Niu, J., Bao, Y. & Hu, L., *Evidence of Superoxide Radical Contribution to Demineralization of Sulfamethoxazole by Visible-Light-Driven $Bi_2O_3/Bi_2O_2CO_3/Sr_6Bi_2O_9$ Photocatalyst*, Journal of Hazardous Materials, **262**, pp. 812-818, Sep. 2013.

[4] Gong, H. & Chu, H., *Photodegradation of Sulfamethoxazole with a Recyclable Catalyst*, Industrial & Engineering Chemistry Research, **54**, pp. 12763-12769, Dec. 2015.

[5] Saputera, W.H., Amri, A.F., Daiyan, R. & Sasongko, D., *Photocatalytic Technology for Palm Oil Mill Effluent (POME) Wastewater Treatment: Current Progress and Future Perspective*, Materials, **14**, 2846, May. 2021.

[6] Saputera, W.H., Amri, A.F., Mukti, R.R., Suendo, V., Devianto, H. & Sasongko, D., *Photocatalytic Degradation of Palm Oil Mill Effluent (POME) Waste Using $BiVO_4$ Based Catalysts*, Molecules, **26**, 6225, Oct. 2021.

[7] Putri, R.M., Almunadya, N.S., Amri, A.F., Afnan, N.T., Nurachman, Z., Devianto, H. & Saputera, W.H., *Structural Characterization of Polycrystalline Titania Nanoparticles on C. striata Biosilica for Photocatalytic POME Degradation*, ACS Omega, **7**, pp. 44047-44056, Nov. 2022.

DOI: 10.5614/j.eng.technol.sci.2024.56.2.7

[8] Bhachu, D.S., Moniz, S.J.A., Sathasivam, S., Scanlon, D.O., Walsh, A. Bawaked, S.M., Mokhtar, M., Obaid, A.Y., Parkin, I.P., Tang, J. & Carmalt, C.J., *Bismuth Oxyhalides: Synthesis, Structure and Photoelectrochemical Activity*, Chemical Science, **7**(8), pp. 4832-4841, Mar. 2016.

[9] He, R., Cao, S., Zhou, P. & Yu, J., *Recent Advances in Visible Light Bi-Based Photocatalysts*, Chinese Journal of Catalysis, **35**(7), pp. 989-1007, Jul. 2014.

[10] Li, Y., Jiang, H., Wang, X., Hong, X. & Liang, B., *Recent Advances in Bismuth Oxyhalide Photocatalysts for Degradation of Organic Pollutants in Wastewater*, RSC Advances, **11**, pp. 26855-26875, Aug. 2021.

[11] Lv, X., Leung, F., Lam, Y., & Hu, X., *A Review on Bismuth Oxyhalide (BiOX, X= Cl, Br, I) Based Photocatalysts for Wastewater Remediation*, **2**, 839072, Apr. 2022.

[12] Wei, W., Gong, H., Sheng, L., Wu, H., Zhu, S., Feng, L., Li, X. & You, W., *Highly Efficient Photocatalytic Activity and Mechanism of Novel Er^{3+} and Tb^{3+} Co-Doped BiOBr/g-C_3N_5 Towards Sulfamethoxazole Degradation*, Ceramics International, **47**, pp. 24062-24072, May. 2021.

[13] Yang, Y., Zhang, C., Lai, C., Zeng, G., Huang, D., Cheng, M., Wang, J., Chen, F., Zhou, C. & Xiong, W., *BiOX (X = Cl, Br, I) Photocatalytic Nanomaterials: Applications for Fuels and Environmental Management,* Advances in Colloid Interface Science, **254**, pp. 76-93, Mar. 2018.

[14] Zeng, X., Wan, Y., Gong, X. & Xu, Z., *Additive Dependent Synthesis of Bismuth Oxybromide Composites for Photocatalytic Removal of The Antibacterial Agent Ciprofloxacin and Mechanism Insight*, RSC Advances. **7** (58), pp. 36269-36278, Jul. 2017.

[15] Yu, C., Cao, F., Li, G., Wei, R., Yu, J.C., Jin, R., Fan, Q. & Wang, C., *Novel Noble Metal (Rh, Pd, Pt)/ BiOX (Cl, Br, I) Composite Photocatalysts with Enhanced Photocatalytic Performance in Dye Degradation*, Separation and Purification Technology,**120**, pp. 110-122, Oct. 2013.

[16] Gao, M., Zhang, D., Pu, X., Li, H., Lv, D., Zhang, B. & Shao, X., *Facile Hydrothermal Synthesis of Bi/BiOBr Composites with Enhanced Visible-Light Photocatalytic Activities for The Degradation of Rhodamine B*, Separation and Purification Technology, **154**, pp. 211-216, Sep. 2015.

[17] Zhang, X., Ji, G., Liu, Y, Zhou, X., Zhu, Y., Shi, D., Zhang, P., Cao, X. & Wang, B., *The Role of Sn in Enhancing the Visible-Light Photocatalytic Activity of Hollow Hierarchical Microspheres of the Bi/BiOBr Heterojunction*, Physical Chemistry Chemical Physics, **17**(12), pp. 8078-8086. Feb. 2015.

[18] Zheng, C., Cao, C. & Ali, Z., *In Situ Formed Bi/BiOBr$_x$I$_{1-x}$ Heterojunction of Hierarchical Microspheres for Efficient Visible Light Photocatalytic Activity*, Physical Chemistry Chemical Physics, **17**(20), pp. 13347-13354, Apr. 2015.

[19] Cao, F., Wang, J., Wang, Y., Zhou, J., Li, S., Qin, G. & Fan, W., *An In Situ Bi-Decorated BiOBr Photocatalyst for Synchronously Treating Multiple Antibiotics in Water*, Nanoscale Advances, **1**(3), pp. 1124-1129. Dec. 2018.

[20] Shi, X., Chen, X., Chen, X., Zhou, S., Lou, S., Wang, Y. & Yuan, L., *PVP Assisted Hydrothermal Synthesis of BiOBr Hierarchical Nanostructures and High Photocatalytic Capacity*, Chemical Engineering Journal, **222**, pp. 120-127. Feb. 2013.

[21] Wei, Z., Dong, X., Zheng, N., Wang, Y., Zhang, X. & Ma, H*., Novel Visible-Light Irradiation Niobium-Doped BiOBr Microspheres with Enhanced Photocatalytic Performance*, Journal of Materials Science, **55**, pp. 16522-16532. Sep. 2020.

[22] Długosz, M., Zmudzki, P., Kwiecień, A., Szczubiałka, K., Krzek, J. & Nowakowska, M., *Photocatalytic Degradation of Sulfamethoxazole in Aqueous Solution Using a Floating TiO_2-Expanded Perlite Photocatalyst*, Journal of Hazardous Materials, **298**, pp. 146-153. May. 2015.

[23] Xu, W., Lyu, F., Bai, Y., Gao, A., Feng, J., Cai, Z. & Yin, Y., *Porous Cobalt Oxide Nanoplates Enriched with Oxygen Vacancies for Oxygen Evolution Reaction*, Nano Energy, **43**, pp. 110-116. Nov. 2017.

[24] Kleja, D.B., Gustafsson, J.P., Kessler, V. & Persson, I., *Bismuth(III) Forms Exceptionally Strong Complexes with Natural Organic Matter*, Environmental Science & Technology, **56**(5), pp. 3076-3084. Feb. 2022.

[25] Hu, X., Zhao, M., Zheng, W. & Zhu, J., *Preparation, Characterization, and Photocatalytic Performance of Ag/BiOBr $_{0.85}$I$_{0.15}$ Nanocomposites*, Materials, **15**, 6022. Aug. 2022.

[26] Wang, Q., Liu, Z., Liu, D., Liu, G., Yang, M., Cui, F. & Wang, W., *Ultrathin Two-Dimensional BiOBr$_x$I$_{1-x}$ Solid Solution with Rich Oxygen Vacancies for Enhanced Visible-Light-Driven Photoactivity in Environmental Remediation*, Applied Catalysis B: Environmental, **236**, pp. 222-232. May. 2018.

[27] Saddique, Z., Imran, M., Javaid, A., Latif, S., Hussain, N., Kowal, P. & Boczkaj, G., *Band Engineering of BiOBr Based Materials for Photocatalytic Wastewater Treatment via Advanced Oxidation Processes (AOPs) – A Review*, Water Resources and Industry, **29**, 100211, Apr. 2023.

[28] Zhou, L., Zhang, W., Chen, L. & Deng, H., *Z-Scheme Mechanism of Photogenerated Carriers for Hybrid Photocatalyst $Ag_3PO_4/G\text{-}C_3N_4$ in Degradation of Sulfamethoxazole*, Journal of Colloid and Interface Science, **487**, pp. 410-417. Oct. 2016.

[29] Jiang, R., Wu, D., Lu, G., Yan, Z., Liu, J., Zhou, R. & Nkoom, M., *Fabrication of Fe_3O_4 Quantum Dots Modified $BiOCl/BiVO_4$ p-n Heterojunction to Enhance Photocatalytic Activity for Removing Broad-Spectrum Antibiotics Under Visible Light*, Journal of the Taiwan Institute of Chemical Engineers, **96**, pp. 681-690. Jan. 2019.

[30] Bao, Y., Lim, T.T., Goei, R., Zhong, Z., Wang, R. & Hu, X., *One-Step Construction of Heterostructured Metal-Organics@Bi_2O_3 with Improved Photoinduced Charge Transfer and Enhanced Activity in Photocatalytic Degradation of Sulfamethoxazole Under Solar Light Irradiation*, Chemosphere, **205**, pp. 396-403. Apr. 2018.

[31] Hoang, D.H., Hang, T.T., Thuy, N.T.M., Thu, B.T., Hoi, B. V. & Huyen, T.T.T., *Degradation of Antibiotic Sulfamethoxazole in Aqueous Media by UVA/TiO_2 Pure-Brookite Photocatalysis*, Vietnam Journal of Science and Technology, **60**(2), pp. 225-236. Mar. 2022

[32] Lu, C.S., Tsai, H.Y., Shaya, J., Golovko, V.B., Wang, S.Y., Liu, W.J. & Chen, C.C., *Degradation of Sulfamethoxazole in Water by $AgNbO_3$ Photocatalyst Mediated by Persulfate*, RSC Advances. **12**(46), pp. 29709-29718. Oct. 2022.

[33] Wu, X., Ng, Y.H., Saputera, W.H., Wen, X., Du, Y., Dou, S.X., Amal, R. & Scott, J., *The Dependence of Bi_2MoO_6 Photocatalytic Water Oxidation Capability on Crystal Facet Engineering*, ChemPhotoChem, **3**, pp. 1246-1253. Aug. 2019.

Manuscript Received: 18 July 2023
1st Manuscript Revision Received: 1 January 2024
2nd Manuscript Revision Received: 4 March 2024
Accepted Manuscript: 02 April 2024